Color calibration of remote sensing imagery based on automatic classification and color space transformation

CHEN Xu, LIN Hong, QIANG Zhen-ping

Computer & Information Science Department, *Southwest Forestry University*, *Yunnan Kunming* 650224, *China*

Abstract: The remote sensing images captured at different time may be quite different in color, brightness because of various atmospheric conditions, seasonal changes in vegetation characteristics and other reasons. These differences not only cause great impact on subsequent image classification and change detection, but also bring difficulties in remote sensing image mosaicking. This paper presents a color calibration method based on remote sensing automatically classification and $l\alpha\beta$ color space transformation. Multi-images mosaic with ETM captured at different time are experimented by applying this method. The results of experiments show that color calibration method can calibrate difference of color and brightness in images caused by the different time more effectively than conventional methods, such as overlapping zone calibration and histogram matching. So it can improve the accuracy of follow-up image classification and change detection, as well as the remote sensing images mosaicking effect.

Key words: remote sensing, color calibration, mosaicking, color space transformation

CLC number: TP751.1 **Document code:** A

1 INTRODUCTION

Nowadays, remote sensing has been used as the primary method of large area real-time geostationary observation. However, besides the effects of the sun, the atmospheric conditions and satellites parameters, seasonal changes in vegetation characteristics (such as the color changes of forest with seasonal changes) would also cause the differences in color and brightness among different remote sensing images. The commonly used method to identify these differences is to obtain statistic parameters through samples taken from the fixed spots in the overlapping zone of the images so as to establish the Overlapping Zone Statistical Linearity Models to calibrate the data (Canty *et al.*, 2004; Du *et al.*, 2001; Du *et al.*, 2002; Furby & Campbell, 2001; Olthof *et al.*, 2005a; Olthof *et al.*, 2005b; Chen *et al.*, 2005; Zhang *et al.*, 2006). The premise of this method is the statistical distributing of the whole image can be respresented by that of the overlapping zone. The study on this method generally focuses on the collecting of sample data and the choosing of linear models. However, the limitations of this method are obvious. Firstly, the division of single image and the overlapping zone do not take the composing of the real surface features into account. The histograms of real surface features might be composed of multi-peaks, which cannot be simulated sufficiently in linearity models. Secondly, there are certain correlations between collecting wave bands of remote sensing satellites and between three color channels generating RGB images. And the modification of any band or channel will have influence on others. Therefore, this method can not show the clear results to calibrate the color differences of images caused by seasonal changes. In this paper, a color calibration method based on remote sensing auto-classification and $l\alpha\beta$ color space transformation is presented. The application of remote sensing auto-classification and $l\alpha\beta$ (Ruderman *et al.*, 1998) color space transformation instead of single linearity model produce better color calibration effects. Meanwhile, satisfactory simulation of remote sensing image data distributing can be achieved, and the influence caused by the correlations of bands and channels can be avoided.

2 METHOD

The flow diagram in Fig. 1 is illustrating the color calibration method based on remote sensing auto-classification and $l\alpha\beta$ color space transformation:

2.1 Atmosphere calibration

The remote sensing images of different atmospheric conditions would show a large variety in color and brightness, which would cause the distortion in the following calibration. Therefore, the atmosphere calibration should be done before the color and brightness calibration.

The atmosphere calibration could be divided into two groups, namely the absolute calibration and the relative calibration (Danaher *et al.*, 2001). The former can accurately calibrate the influences of the atmosphere on radiation transmission. However, the absolute calibration cannot be effectively applied in many cases because of the hardness to get the exact atmospheric optical parameters when the images are captured. The

Received: 2008-02-20; **Accepted**: 2008-04-23

Foundation: Key Scientific Research Projects Foundation of Southwest Forestry University (No. 110712).

First author biography: CHEN Xu (1973—), Male, Lecturer. His research interests include remote sensing image processing, 3S technology application, etc. He authored/co-authored over 8 technical papers. E-mail: chenxu_gis@yahoo.com.cn

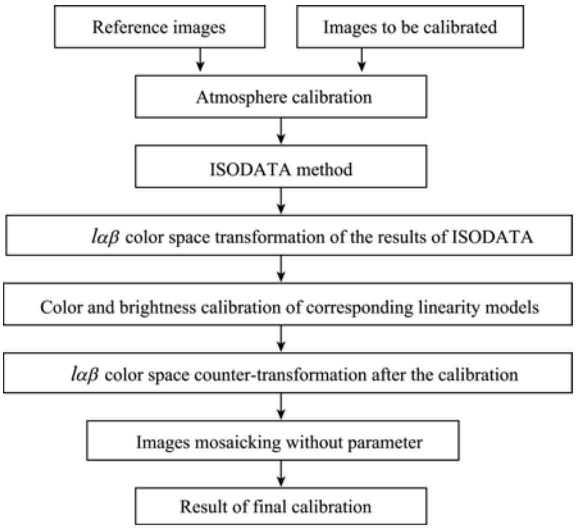

Fig. 1 Color calibration method flow diagram

parameters needed in relative calibration all come from the images, such as DOS (Dark Object Subtraction) Methods, which are applied widely for their convenience and effectiveness (Spanner *et al*., 1990; Ekstrand, 1994; Jakubauskas, 1996; Huguenin *et al*., 1997). DDV (Dense Dark Vegetation) Method in DOS Methods is introduced in this paper to complete the atmosphere calibration (Song *et al*., 2001). The formulas of this method are as follows:

$$L_{\mathrm{p}} = G \times \mathrm{DN}_{\min} + B - 0.01 E_0 \cos(\theta_z)/\pi \tag{1}$$

$$\rho = \frac{\pi(L_{\mathrm{sat}} - L_{\mathrm{p}})}{E_0 \cos(\theta_z)} \tag{2}$$

where L_{sat} is the at-satellite radiance, L_{p} is the path radiance, θ_z is the solar zenith angle, and E_0 is the exoatmospheric solar constant.

2.2 ISODATA

The foundation of the Statistical Distributing Correlation Method is that the correlation shown in color distributing and composing of two images. The large diversity of surface features will cause the large variety in color composing and distributing, which will be represented by multi-peaks in data histograms. The data distributing of multi-peaks is different, so color calibration is hard to complete only by linearity statistical methods. In color calibration, both the coordination of the colors in the whole image and the particularity of different surface features should be taken into account. To achieve better calibration correlation of various surface features in the whole image, remote sensing auto-classification methods are introduced in this study and images are classified according to the number of the peaks in the histograms firstly. The most commonly used method is ISODATA, which works without transcendent knowledge. According to the ISODATA method, certain samples are selected as clustering centers, and then other samples will be gathered around the centers under the rule of the minimal distance, hence form the original clustering. Then the result of the original clustering will be judged whether it is fit to the acquirements. If it is not, the clustering will be divided and combined iteratively to form a new clustering center (the clustering center is determined by the iterative operation on the mean value of the samples) to meet the acquirement and complete the clustering classification.

2.3 $l\alpha\beta$ color space transformation of the results of ISODATA

$l\alpha\beta$ color space put forward by Ruderman *et al.* (1998)is introduced in this paper in order to get rid of the influence of the correlations between the channels from which images obtained and the three channels of RGB color space. The major characteristic of the color space is the minimal correlation influence of the channels in most natural scenes images. The color space provides three de-correlated, principal channels corresponding to an achromatic luminance channel l and two chromatic channels α and β, which roughly correspond to yellow-blue and red-green opponent channels.

$l\alpha\beta$ color space is a variety of cone color space *LMS*, so *RGB* color space images should be changed into *LMS* color space ones first. The transformation formula is as follows:

$$\begin{bmatrix} L \\ M \\ S \end{bmatrix} = \begin{bmatrix} 0.3811 & 0.5783 & 0.0402 \\ 0.1967 & 0.7244 & 0.0782 \\ 0.0241 & 0.1288 & 0.8444 \end{bmatrix} \begin{bmatrix} R \\ G \\ B \end{bmatrix} \tag{3}$$

After the transformation, there will be large skew in statistical distributing of the image data, which can be eliminated by the transformation from *LMS* color space into logarithm *LMS* space. The transformation formulas are as follows:

$$\begin{aligned} L' &= \log L \\ M' &= \log M \\ S' &= \log S \end{aligned} \tag{4}$$

Then logarithm *LMS* space images can be changed into $l\alpha\beta$ color space images through following formula:

$$\begin{bmatrix} l \\ \alpha \\ \beta \end{bmatrix} = \begin{bmatrix} \frac{1}{\sqrt{3}} & 0 & 0 \\ 0 & \frac{1}{\sqrt{6}} & 0 \\ 0 & 0 & \frac{1}{\sqrt{2}} \end{bmatrix} \begin{bmatrix} 1 & 1 & 1 \\ 1 & 1 & -2 \\ 1 & -1 & 0 \end{bmatrix} \begin{bmatrix} L' \\ M' \\ S' \end{bmatrix} \tag{5}$$

2.4 Color and brightness calibration of corresponding linearity models

By calculating the means and variances of every class in the reference images and images to be calibrated after the $l\alpha\beta$ color space transformation respectively, the data distributing of the images to be calibrated can be matched on that of the reference images by applying linearity models (Hertzmann, 2001). The formula is as follows:

$$Y_i(p)' = \frac{\sigma_{i2}}{\sigma_{i1}}(Y_i(p) - \mu_{i1}) + \mu_{i2} \tag{6}$$

where μ_{i2}, σ_{i2}, μ_{i1} and σ_{i1} are the means and variances of class i of the reference images and images to be calibrated respectively. $Y_i(p)$ is the value of a pixel in the class i of the images to be calibrated after $l\alpha\beta$ color space transformation, and $Y_i(p)'$ is the value of a pixel after the calibration. Formula 6 should be applied in images of all classes to achieve the color and brightness calibration.

Furthermore, we compute the distance to the center of each of the source clusters and divide it by the cluster's standard deviation so as to get rid of images mosaic lines caused by different standard deviation of different classes. This division is required to compensate for different cluster sizes. We blend the scaled and shifted pixels with weights inversely proportional to these normalized distances, yielding the final image. This approach can make the color coordination in the whole image.

2.5 $l\alpha\beta$ color space counter-transformation after the calibration

The results of the calibration should be changed into *RGB* color space to continue images mosaicking without parameter (original data) to obtain the final calibration results. The formulas are as follows:

$$\begin{bmatrix} L' \\ M' \\ S' \end{bmatrix} = \begin{bmatrix} 1 & 1 & 1 \\ 1 & 1 & -1 \\ 1 & -2 & 0 \end{bmatrix} \begin{bmatrix} \frac{\sqrt{3}}{3} & 0 & 0 \\ 0 & \frac{\sqrt{6}}{6} & 0 \\ 0 & 0 & \frac{\sqrt{2}}{2} \end{bmatrix} \begin{bmatrix} l \\ \alpha \\ \beta \end{bmatrix} \tag{7}$$

$$\begin{aligned} L &= 10^{L'} \\ M &= 10^{M'} \\ S &= 10^{S'} \end{aligned} \tag{8}$$

$$\begin{bmatrix} R \\ G \\ B \end{bmatrix} = \begin{bmatrix} 4.4679 & -3.5873 & 0.1193 \\ -1.2186 & 2.3809 & -0.1624 \\ 0.0497 & -0.2439 & 1.2045 \end{bmatrix} \begin{bmatrix} L \\ M \\ S \end{bmatrix} \tag{9}$$

3 EXPERIMENTS AND RESULTS

Two ETM images were experimented with the method suggested in this paper. The orbit numbers of these two images are p124r045 and p124r046, and the time to capture them is October 30th, 2000 and April 8th, 2001 respectively. The original image and the calibrated image are presented in Fig. 2, in which (a) is the reference image, (b) is the image to be calibrated, (c) is the result of overlapping zone calibration, and (d) is the result of the calibration by using the method suggested in this paper.

Fig. 2 indicates the existence of large differences in the color and the brightness of both the vegetation and the water between the reference image and the image to be calibrated. In the reference image, the dark green of the autumn and the peak green of the spring in the image are to be calibrated. Using overlapping zone calibration method produces little effect in this case, and better result is achieved by the method suggested in this paper.

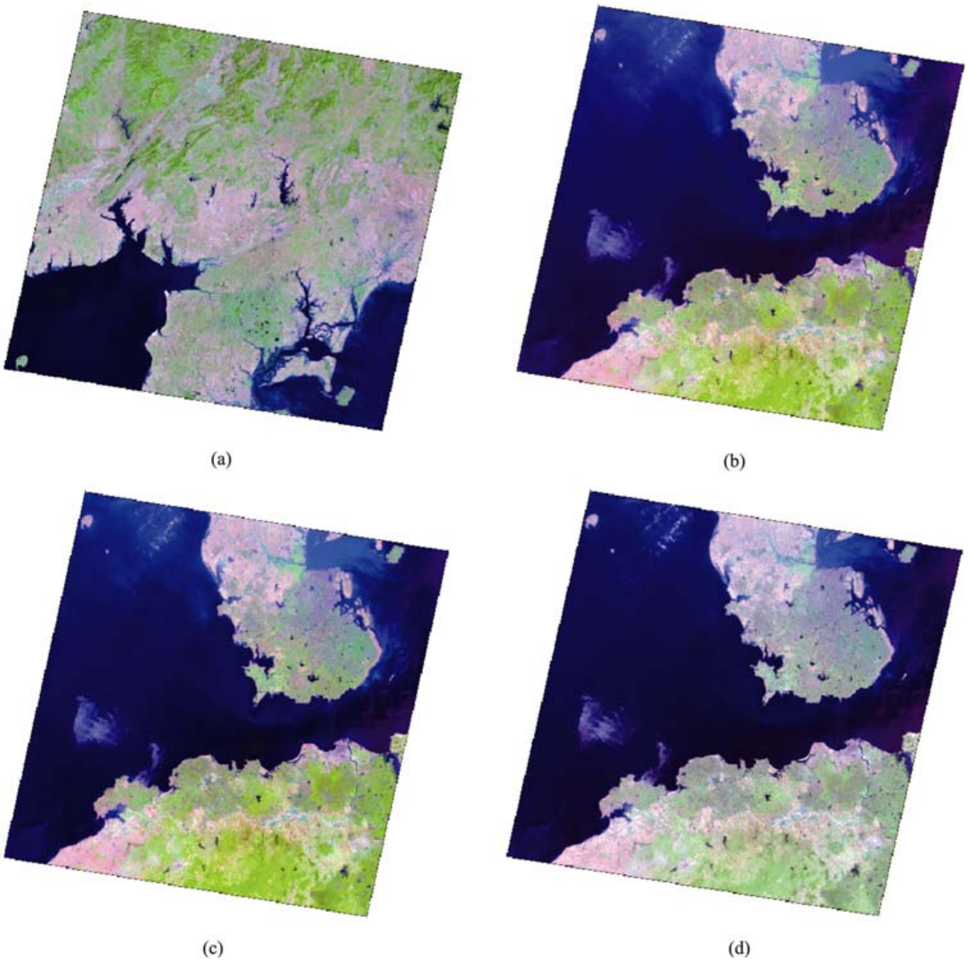

Fig. 2 Results of color calibration

(a) The reference image; (b) The image to be calibrated; (c) The result of overlapping zone calibration; (d) The result of calibration using the method suggested in this paper

In Fig. 3, DN histograms before and after image calibration, we can find that both the overlapping zone calibration method and the method suggested in this paper changed the histograms and make them similiar to the reference image and normalize as the first band. However, as to the third band with multi-peaks, the overlapping zone calibration method generates little effect both on the first peak representing the water and the second peak representing the vegetation; with the method suggested in this paper the second peak representing the vegetation has been calibrated satisfactorily, but some parts of the first peak representing the water seem to be over-calibrated.

According to Table 1, the statistics comparison of images before and after color calibration, as to the means and variances of different bands of the image to be calibrated, both the overlapping zone calibration method and the method suggested in this paper have modified the image to be calibrated. According to the results of the histograms, the overlapping zone calibration method attempts to calibrate the statistical distributing of different bands of the image to be calibrated to that of the reference image. However, due to the correlations of different bands, the data distributing after the overlapping zone calibration differ greatly from both that of the reference image and that of the overlapping zone of the reference image. The data distributing on different bands after the calibration method suggested in this paper are similar to that of the reference image.

The color calibration method suggested in this paper has been applied in remote sensing multi-images mosaic experiment. The original images and the results are showed in Fig. 4 to Fig. 6. From Fig. 4, we can find that there are large differences both in color and brightness in original images, especially in the images with water. The mosaicking by histogram matching cannot achieve significant effect, which is demonstrated in Fig. 5. The mosaic line between images with water and other images is distinct, and the two images on the lower part of Fig. 5 are over-calibrated. Fig. 6 shows that the method suggested in this paper can obtain better effect. There is no distinct mosaic line between images with water and other images. The two images on the lower part of the figure are not over-calibrated, and better color harmony is achieved. Compared with the results of the histogram matching method, the method suggested in this paper can obtain better results in color and brightness.

4 CONCLUSION

The color calibration method based on remote sensing automatically classification and $l\alpha\beta$ color space transformation can be summarized as the following: According to the number of the peak in the images' histogram, images are classified and fit for linearity statistical methods. At the same time, the $l\alpha\beta$ color space was used to get rid of the influences of the correlations between the three channels of *RGB* color space and the channels from which images are obtained. With weights inversely proportional, the mosaic image's color is in harmony

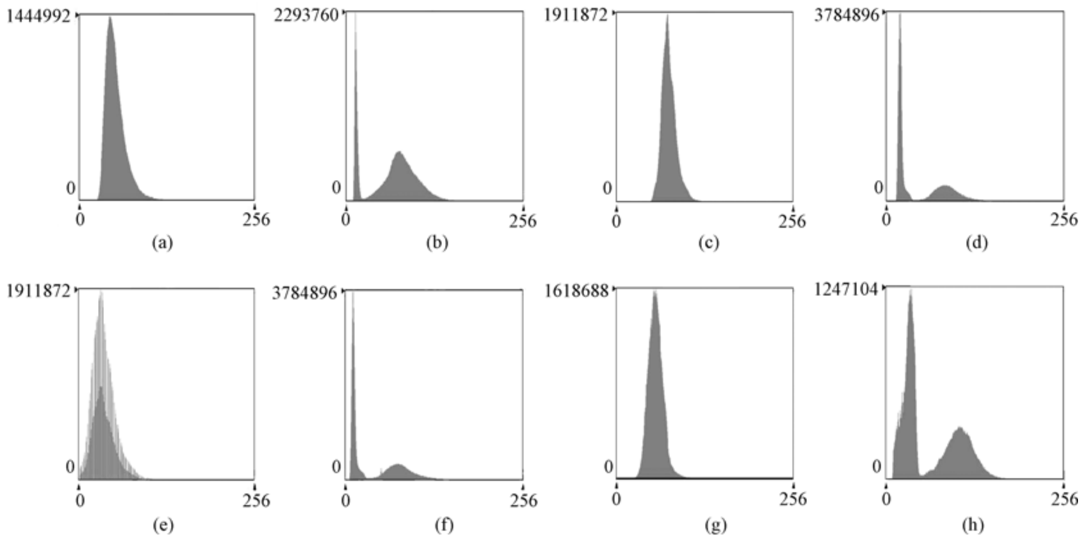

Fig. 3 DN Histograms before and after image calibration

(a) The first band of the reference image; (b) The third band of the reference image; (c) The first band of the calibrated image; (d) The third band of the calibrated image; (e) The first band of the calibration result using the image's overlap zone; (f) The third band of the calibration result by using the image's overlap zone; (g) The first band of the calibration result by the method suggested in this paper; (h) The third band of the calibration result by the method suggested in this paper

Table 1 Statistics comparison of images before and after color calibration

Statistics variable	Band	Reference image	Image to be calibrated	Overlapping zone in reference image	Overlapping zone in image to be calibrated	The result of overlapping zone calibration method	The result of the calibration method suggested in this paper
Mean	1	39.548	75.852	55.565	63.719	36.794	39.025
	2	58.788	46.032	31.866	38.781	37.751	58.248
	3	67.879	50.932	36.344	47.283	42.544	67.787
Variances	1	11.537	11.433	14.623	11.453	17.909	12.365
	2	26.870	24.240	26.692	28.751	34.062	25.607
	3	39.745	39.581	36.676	42.850	39.136	40.598

Fig. 4 The original images overlapping

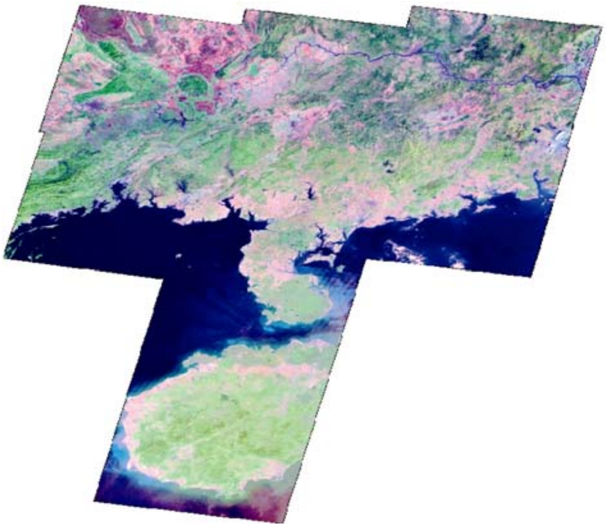

Fig. 5 The mosaic result of histogram matching

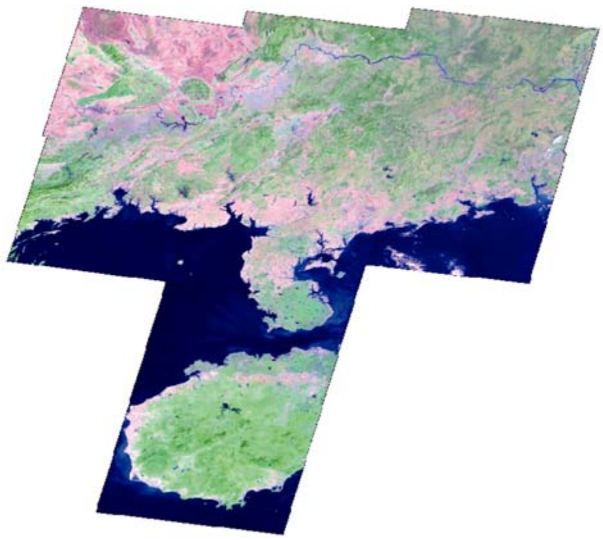

Fig. 6 The mosaic result using the method suggested in this paper

and has few mosaic lines. The experimental results show that this method can calibrate differences of color and brightness in images of different time. Consequently, it can obtain satisfactory results on subsequent image classification and change detection.

REFERENCES

Canty M J, Nielsen A A and Schmidt M. 2004. Automatic radiometric normalization of multitemporal satellite imagery. *Remote Sensing of Environment*, **91**: 441—451

Chen X X, Vierling L and Deering D. 2005. A simple and effective radiometric correction method to improve landscape change detection across sensors and across time. *Remote Sensing of Environment*, **98**:63—79

Danaher T, Wu X L and Campbell N. 2001. Bi-directional reflectance distribution function approaches to radiometric calibration of landsat ETM+ imagery. *Geoscience and Remote Sensing Symposium*, **6**: 2654—2657

Du Y, Cihlar J, Beaubien J and Latifovic R. 2001. Radiometric normalization, compositing, and quality control for satellite high resolution image mosaics over large areas. *IEEE Transactions on Geoscience and Remote Sensing*, **39**(3): 623—634

Du Y, Teillet P M and Cihlar J. 2002. Radiometric normalization of multitemporal high-resolution satellite images with quality control for land cover change detection. *Remote Sensing of Environment*, **82**:123—134

Ekstrand S. 1994. Assessment of forest damage with landsat TM: correction for varying forest stand characteristics. *Remote Sensing of Environment*, **47**: 291—302

Furby S L and Campbell N A. 2001. Calibrating images from different dates to ‘like-value’ digital counts. *Remote Sensing of Environment*, **77**: 186—196

Hertzmann A, Jacobs C E, Oliver N, Curless B and Salesin D H. 2001. Image analogies. *ACM Siggraph*, 327—340

Huguenin R L, Karaska M A, Blaricom D V and Jensen J R. 1997. Subpixel classification of bald cypress and tupelo gum trees in thematic mapper imagery. *Photogramm. Eng. Remote Sens*. **63**(6): 717—725

Jakubauskas M E. 1996. Thematic mapper characterization of lodgepole pine seral stages in Yellowstone Nationa Park, USA. *Remote Sensing of Environment*, **56**: 118—132

Olthof I, Butson C and Fraser R. 2005a. Signature extension through space for northern landcover classification: A comparison of radiometric correction methods. *Remote Sensing of Environment*, **95**: 290—302

Olthof I, Darren Pouliot, Richard Fernandes and Rasim Latifovic. 2005b. Landsat-7 ETM+ radiometric normalization comparison for northern mapping applications. *Remote Sensing of Environment*, **95**: 388—398

Ruderman D L, Cronin T W and Chiao C C. 1998. Statistics of cone responses to natural images: implications for visual coding. *Optical Society of America*, **15**(8): 2036—2045

Song Conghe, Curtis E Woodcock, Karen C Seto, Mary Pax Lenney and Scott A Macomber. 2001. Classification and change detection using Landsat TM Data: when and how to correct atmospheric effects? *Remote Sensing of Environment*, **75**: 230—244

Spanner M A, Pierce L L, Peterson D L and Running S W. 1990. Remote sensing of temperate coniferous forest leaf area index: the influence of canopy closure, understory vegetation and background reflectance. *Int. J. Remote Sensing*, **11**(1): 95—111

Zhang P Q, Yu X C, Liu Z, Li J S and Wan G. 2006. A study on relative radiometric correction of multitemporal remote sensing images. *Journal of Remote Sensing*, **10**(3): 339—344

基于自分类和颜色空间变换的遥感图像色彩校正方法

陈　旭，林　宏，强振平

西南林学院 计算机与信息科学系，云南 昆明　650224

摘　要：提出了一种基于遥感自动分类和 $l\alpha\beta$ 颜色空间变换的色彩校正方法，并用此方法对不同时间的 ETM 遥感图像进行了多景色彩校正后的拼接实验。实验结果显示，相对于重叠区域校正、直方图匹配等常规方法，该方法能够很好地校正不同获取时间所导致的景间颜色、亮度差异，提高遥感图像后续分类、变化检测的准确性以及多景遥感图像的拼接效果。

关键词：遥感，色彩校正，拼接，颜色空间变换

中图分类号：TP751.1　　文献标识码：A

1　引　言

卫星遥感已成为当今大面积实时对地监测的最主要手段。但是，不同时间获取的卫星遥感图像，除了受到太阳、大气和卫星参数等方面的影响外，还可能因为气候季节的变化(如森林颜色随季节的变化)造成景间颜色、亮度的不一致。目前解决景间颜色、亮度差异的主要方法是通过在景间重叠部分的固定特征点中抽取样本并计算统计参数，利用重叠区域统计线性模型校正方法使各景图像数据在统计分布上达到基本一致来实现(Canty 等，2004; Du 等，2001; Du 等，2002; Furby & Campbell, 2001; Olthof 等, 2005a, 2005b; Chen 等, 2005; Zhang 等, 2006)。这一方法的基本前提是重叠区域的统计分布可以代表整幅图像的统计分布，对这一方法的研究主要涉及样本数据集与线性模型的选取。然而，这一方法的缺陷是显而易见的。其一，由于遥感图像单景大小和景间重叠区域大小的划分并没有考虑实际地物组成情况，实际地物的组成在直方图中可能由多个峰组成，线性模型不能很好的模拟整个数据分布。其二，遥感卫星的各个采集波段之间以及生成的 *RGB* 图像的 3 个颜色通道之间存在一定的相关性，对任意波段或通道的修改会影响到其他波段或通道，因季节变化等原因引起的较大颜色差异问题使用这一方法很难获得好的效果，这在很大程度上限制了重叠区域线性模型校正方法的使用。为此，本文引入了数字图像处理中的颜色空间变换技术，结合遥感自分类技术提出了一种基于遥感自分类和颜色空间变换的色彩校正方法。本方法通过遥感自分类和进行 $l\alpha\beta$ (Ruderman 等, 1998)颜色空间变换，解决了单一线性模型不能很好模拟整幅遥感图像数据分布的缺陷和消除了各个波段之间的相关性，取得了很好的色彩校正效果。

2　方　法

本文提出的基于遥感自分类和颜色空间变换的色彩校正方法的处理流程如图 1。

2.1　大气校正

由于遥感图像在成像时容易受到大气的影响，不同的大气情况会对图像的亮度和颜色分布产生影响，从而导致后续的校正偏差。因此，在对图像进行亮度和颜色校正时需要首先对图像进行大气校正。

收稿日期：2008-02-20；修订日期：2008-04-23

基金项目：西南林学院重点科研基金项目资助(项目编号：110712)。

第一作者简介：陈旭(1973—　)，男，讲师，中山大学 3S 技术应用博士毕业。研究方向为遥感图像处理、3S 技术应用等领域，发表论文 8 篇。E-mail: chenxu_gis@yahoo.com.cn。

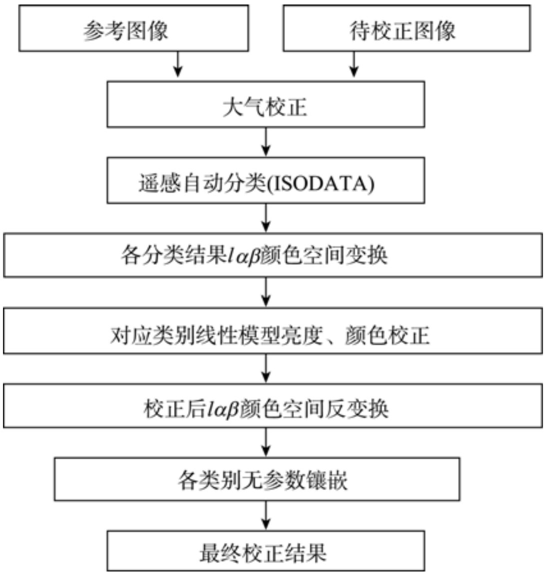

图 1 色彩校正方法流程图

通常大气校正分为绝对校正和相对校正(Danaher 等, 2001)。前者能够较准确的校正大气对辐射传输的影响，但诸如图像获取时的大气光学参数等校正参数很难甚至是不可能准确获得，因而限制了它的使用。后者的参数来自于图像本身，其中最具代表性的 DOS(dark object subtraction)法因其简单有效而被广泛的使用(Spanner 等, 1990; Ekstrand, 1994; Jakubauskas 1996; Huguenin 等, 1997)。本文选用 DOS 法中的 DDV(dense dark vegetation)方法进行大气校正(Song 等, 2001)，其公式如下:

$$L_{\mathrm{p}} = G \times \mathrm{DN}_{\min} + B - 0.01E_0\cos(\theta_{\mathrm{z}})/\pi \tag{1}$$

$$\rho = \frac{\pi(L_{\mathrm{sat}} - L_{\mathrm{p}})}{E_0\cos(\theta_{\mathrm{z}})} \tag{2}$$

式中，L_{sat}是卫星接收到的辐射值，L_{p}是程辐射，θ_z是太阳天顶角，E_0是大气外的太阳常量。

2.2 遥感自动分类

统计分布一致性方法是以两景图像的颜色分布和组成基本一致为基础的，如果地物组成种类差异较大造成颜色组成和分布差异较大，即在数据直方图上表现为多峰状态，多峰数据分布不同，单一的使用线性统计方法是很难使颜色协调到一致的。色彩校正中，既要考虑图像整体色彩的协调性，又要考虑不同地物种类的特殊性，所以如果图像中地物组成种类差异较大(多峰)，则不能简单使用线性统计分布一致性方法。为了使整个图像中各种地物组成能够有较好的校正一致性，本研究应用遥感自分类方法首先把图像按照直方图中峰的个数分类。遥感自分类中最常用的是非监督分类(ISODATA)，ISODATA 算法是在没有先验知识的情况下进行分类，它先选择若干样本作为聚类中心，按照最小距离准则使其余样本向各中心聚集，从而得到初始聚类，然后判断初始聚类结果是否符合要求，若不符，则将聚类集进行分裂和合并处理，以获得新的聚类中心(聚类中心是通过样本均值的迭代运算来决定的)，再判断聚类结果是否符合要求。如此反复迭代，直到完成聚类划分操作。

2.3 分类结果 $l\alpha\beta$ 颜色空间变换

由于遥感图像获取通道以及常用 RGB 颜色空间 3 个通道之间存在一定的相关性，在各个分类结果色彩校正中，为了消除通道间相关性，本研究选用了 Ruderman 等(1998)提出的 $l\alpha\beta$颜色空间。其特点是这一颜色空间对于大多数自然场景的图像具有通道之间最小的相关性。其中，颜色空间三分量 $l\alpha\beta$分别代表了无色组分，黄-蓝组分和红-绿组分。

$l\alpha\beta$颜色空间是圆锥颜色空间 LMS 的一种变换。所以需要把图像从 RGB 颜色空间转换到 LMS 颜色空间，转换公式为:

$$\begin{bmatrix} L \\ M \\ S \end{bmatrix} = \begin{bmatrix} 0.3811 & 0.5783 & 0.0402 \\ 0.1967 & 0.7244 & 0.0782 \\ 0.0241 & 0.1288 & 0.8444 \end{bmatrix} \begin{bmatrix} R \\ G \\ B \end{bmatrix} \tag{3}$$

图像转换到 LMS 颜色空间后，转换后图像数据的统计分布存在很大的偏移，可通过将 LMS 颜色空间转换到对数 LMS 空间来消除，转换公式为:

$$\begin{aligned} L' &= \log L \\ M' &= \log M \\ S' &= \log S \end{aligned} \tag{4}$$

最后，通过以下的转换公式把图像从对数 LMS 颜色空间转换到 $l\alpha\beta$ 颜色空间，转换公式为:

$$\begin{bmatrix} l \\ \alpha \\ \beta \end{bmatrix} = \begin{bmatrix} \frac{1}{\sqrt{3}} & 0 & 0 \\ 0 & \frac{1}{\sqrt{6}} & 0 \\ 0 & 0 & \frac{1}{\sqrt{2}} \end{bmatrix} \begin{bmatrix} 1 & 1 & 1 \\ 1 & 1 & -2 \\ 1 & -1 & 0 \end{bmatrix} \begin{bmatrix} L' \\ M' \\ S' \end{bmatrix} \tag{5}$$

2.4 线性模型亮度、颜色校正

分别计算 $l\alpha\beta$颜色空间变换后参考图像和待校正图像各个类别的均值和方差。其中，参考图像部分表示为μ_{i2} 和σ_{i2}，待校正图像部分表示为μ_{i1} 和σ_{i1}，

用于代表第 i 个类别的数据分布状况。利用线性模型将待校正图像对应类别的数据分布匹配到参考图像对应类别上(Hertzmann, 2001)，其公式为：

$$Y_i(p)' = \frac{\sigma_{i2}}{\sigma_{i1}}(Y_i(p) - \mu_{i1}) + \mu_{i2} \tag{6}$$

式中，$Y_i(p)$是待校正图像第 i 类 $l\alpha\beta$ 颜色空间变换后像元值，$Y_i(p)'$是校正后第 i 类图像像元值。将式(6)应用于待校正图像的所有类别实现亮度、颜色校正。

另外，为了消除各类别标准方差不一致可能导致的各类别镶嵌时拼接缝的问题，计算各像元对相应类别的中心(均值)的距离，将所得距离除以各个类别的标准方差后作为距离权重参数，利用反向归一化权重方法，将反向归一化距离权重参数乘以各个类别的校正值后求得对应像元的最终校正值，以保证图像整体色彩协调。

2.5　校正后 $l\alpha\beta$颜色空间反变换

最后将校正后各个类别转换回 RGB 空间并进行无参数(原始数据)的镶嵌，获得最终校正结果。$l\alpha\beta$ 颜色空间反变换公式如下：

$$\begin{bmatrix} L' \\ M' \\ S' \end{bmatrix} = \begin{bmatrix} 1 & 1 & 1 \\ 1 & 1 & -1 \\ 1 & -2 & 0 \end{bmatrix} \begin{bmatrix} \frac{\sqrt{3}}{3} & 0 & 0 \\ 0 & \frac{\sqrt{6}}{6} & 0 \\ 0 & 0 & \frac{\sqrt{2}}{2} \end{bmatrix} \begin{bmatrix} l \\ \alpha \\ \beta \end{bmatrix} \tag{7}$$

$$\begin{aligned} L &= 10^{L'} \\ M &= 10^{M'} \\ S &= 10^{S'} \end{aligned} \tag{8}$$

$$\begin{bmatrix} R \\ G \\ B \end{bmatrix} = \begin{bmatrix} 4.4679 & -3.5873 & 0.1193 \\ -1.2186 & 2.3809 & -0.1624 \\ 0.0497 & -0.2439 & 1.2045 \end{bmatrix} \begin{bmatrix} L \\ M \\ S \end{bmatrix} \tag{9}$$

3　实验及结果

首先选用了 2 景 ETM 图像为例对本文提出的方法进行了实验。2 景图像轨道号分别为 p124r045 和 p124r046，获取时间分别为 2000-10-30 和 2001-04-08。原始图及处理结果如图 2。

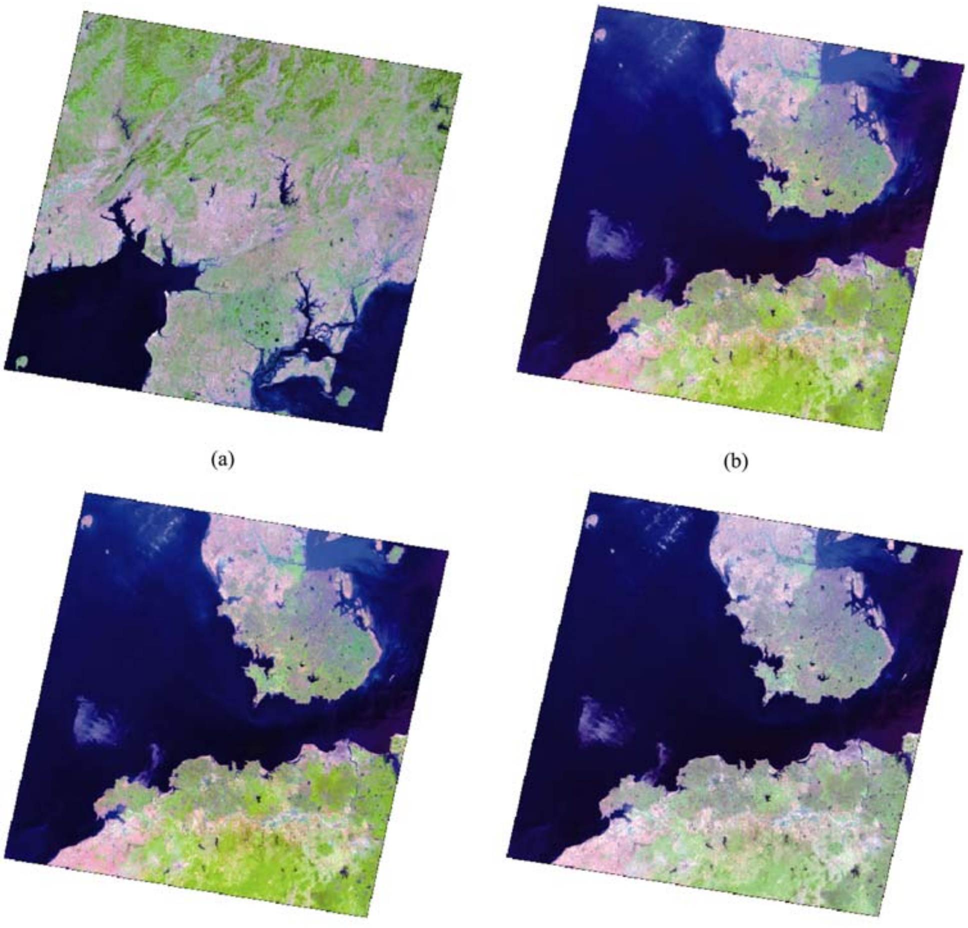

(a)　(b)　(c)　(d)

图 2　本文方法色彩校正结果

(a)参考图像；(b)待校正图像；(c)重叠区域校正结果；(d)本文方法校正结果

从图 2 可以看出，由于季节差异，参考景图像和待校正景图像中植被和水体的颜色与亮度差异较大，参考景图像为秋季的深绿色，而待校正景图像则为春季的嫩绿色。使用重叠区域校正方法对于此类季节所致的色彩差异基本没有效果，而本文提出的方法则较好的校正了 2 景图像之间的色彩差异。

从图 3 的校正前后图像 DN 值直方图中可以看出，在第一波段即单峰波段，重叠区域校正方法和本文方法改动了直方图并使其趋向于参考景图像和正态化。对于多峰的第 3 波段，重叠区域校正方法无论是对代表水域的第 1 个峰还是代表陆地和植被的第 2 个峰基本没有造成影响；而本文提出的方法则很好地校正了代表陆地和植被的第 2 个峰，但同时代表水体的第一个峰则显示了部分水体的过度校正。

从表 1 校正前后图像的均值和方差看，重叠区域校正方法和本文方法对待校正图像各个波段的均值和方差进行了修改。和直方图的结果相似，重叠区域校正方法也试图将待校正图像各个波段数据的统计分布校正到与参考图像一致。但是由于各个波段之间相关性的原因，重叠区域校正结果各个波段的数据分布无论是与参考图像相比较还是和参考图像重叠区域相比较均存在较大差异。而本文提出方法校正结果的数据分布在各个波段上和参考图像十分相似。

应用本文提出的色彩校正方法对多景遥感图像处理结果进行了拼接对比实验，实验原始图和结果如图 4—图 6。从图 4 可以看出，各原始景图像在颜色和亮度上差异很大，特别是含有水域的几景图像差异更大。简单的使用直方图匹配的拼接效果不甚理想，见图 5。其中，含有水域的几景图像和其他景图像之间的拼接缝较为明显，拼接图像下部 2 景图像更是被过度的校正了。而经过本文方法处理后的拼接效果则较为令人满意，见图 6。含有水域的各景和其他景图像之间没有明显的拼接缝，拼接图像下部 2 景不但没有过度校正，而且达到了很好的色彩一致性。本文方法处理后的拼接图像相对于直方图匹配的拼接结果有更好的色彩和亮度一致性，图像更加平滑。

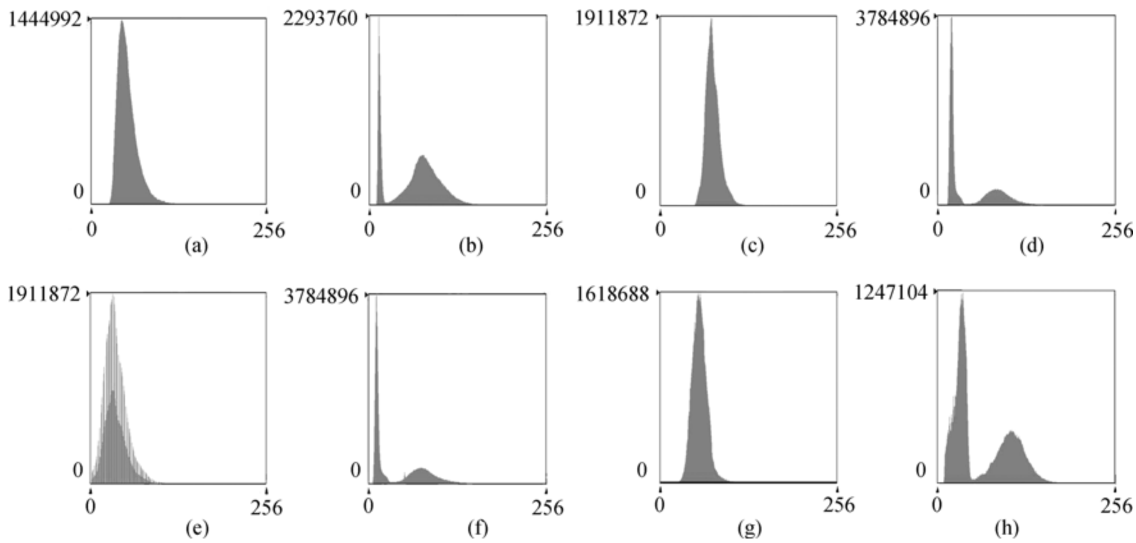

图 3 图像校正前后的 DN 值直方图

(a)参考图第 1 波段;(b)参考图第 3 波段; (c)待校正图第 1 波段; (d)待校正图第 3 波段; (e)重叠区校正图第 1 波段; (f)重叠区校正图第 3 波段; (g)本文方法校正图第 1 波段; (h)本文方法校正图第 3 波段

表 1 色彩校正前后统计值对比

统计值	波段	参考景	待校正景	参考景重叠区	待校正景重叠区	重叠区域校正结果	本文方法校正结果
均值	1	39.548	75.852	55.565	63.719	36.794	39.025
	2	58.788	46.032	31.866	38.781	37.751	58.248
	3	67.879	50.932	36.344	47.283	42.544	67.787
方差	1	11.537	11.433	14.623	11.453	17.909	12.365
	2	26.870	24.240	26.692	28.751	34.062	25.607
	3	39.745	39.581	36.676	42.850	39.136	40.598

图 4　原始图像叠置

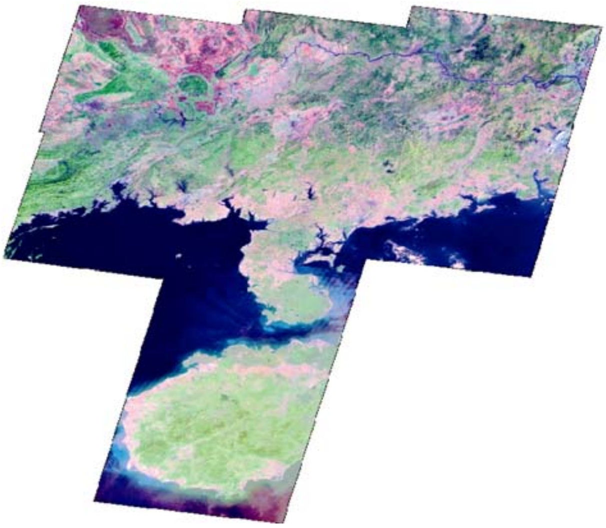

图 5　直方图匹配拼接结果

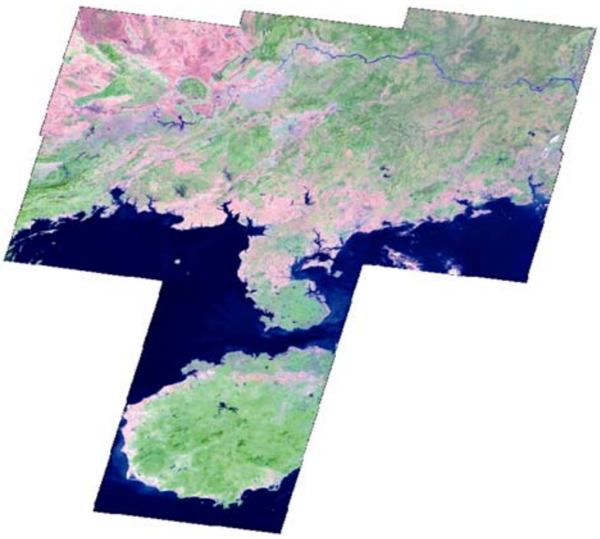

图 6　本研究方法拼接结果

4　结　论

本文所采用的基于遥感自动分类和颜色空间变换的色彩校正方法针对地物组成在图像 DN 值直方图上峰的个数进行了分类，很好地解决了现有的重叠区域校正线性模型存在的缺陷；同时，将具有相关性的波段组合变换到正交的 $l\alpha\beta$空间使各波段的校正相对独立；最后，运用了反向权重的处理方法避免了各个类别镶嵌和重叠区域拼接缝的问题。试验结果显示本方法对因季节变化等原因造成的较大色彩差异的色彩校正取得了很好的效果，能够获得令人满意的遥感图像后续处理结果。

REFERENCES

Canty M J, Nielsen A A and Schmidt M. 2004. Automatic radiometric normalization of multitemporal satellite imagery. *Remote Sensing of Environment*, **91**: 441—451

Chen X X, Vierling L and Deering D. 2005. A simple and effective radiometric correction method to improve landscape change detection across sensors and across time. *Remote Sensing of Environment*, **98**:63—79

Danaher T, Wu X L and Campbell N. 2001. Bi-directional reflectance distribution function approaches to radiometric calibration of landsat ETM+ imagery. *Geoscience and Remote Sensing Symposium*, **6**: 2654—2657

Du Y, Cihlar J, Beaubien J and Latifovic R. 2001. Radiometric normalization, compositing, and quality control for satellite high resolution image mosaics over large areas. *IEEE Transactions on Geoscience and Remote Sensing*, **39**(3): 623—634

Du Y, Teillet P M and Cihlar J. 2002. Radiometric normalization of multitemporal high-resolution satellite images with quality control for land cover change detection. *Remote Sensing of Environment*, **82**:123—134

Ekstrand S. 1994. Assessment of forest damage with landsat TM: correction for varying forest stand characteristics. *Remote Sensing of Environment*, **47**: 291—302

Furby S L and Campbell N A. 2001. Calibrating images from different dates to “like-value” digital counts. *Remote Sensing of Environment*, **77**:186—196

Hertzmann A, Jacobs C E, Oliver N, Curless B and Salesin D H. 2001. Image analogies. *ACM Siggraph*, 327—340

Huguenin R L, Karaska M A, Blaricom D V and Jensen J R. 1997. Subpixel classification of bald cypress and tupelo gum trees in thematic mapper imagery. *Photogramm. Eng. Remote Sens*. **63**(6): 717—725

Jakubauskas M E. 1996. Thematic mapper characterization of lodgepole pine seral stages in Yellowstone Nationa Park, USA.

Remote Sensing of Environment, **56**: 118—132

Olthof I, Butson C and Fraser R. 2005a. Signature extension through space for northern landcover classification: A comparison of radiometric correction methods. *Remote Sensing of Environment*, **95**: 290—302

Olthof I, Darren Pouliot, Richard Fernandes and Rasim Latifovic. 2005b. Landsat-7 ETM+ radiometric normalization comparison for northern mapping applications. *Remote Sensing of Environment*, **95**: 388—398

Ruderman D L, Cronin T W and Chiao C C. 1998. Statistics of cone responses to natural images: implications for visual coding. *Optical Society of America*, **15**(8): 2036—2045

Song Conghe, Curtis E Woodcock, Karen C Seto, Mary Pax Lenney and Scott A Macomber. 2001. Classification and change detection using Landsat TM Data: when and how to correct atmospheric effects? *Remote Sensing of Environment*, **75**: 230—244

Spanner M A, Pierce L L, Peterson D L and Running S W. 1990. Remote sensing of temperate coniferous forest leaf area index: the influence of canopy closure, understory vegetation and background reflectance. *Int. J. Remote Sensing*, **11**(1): 95—111

Zhang P Q, Yu X C, Liu Z, Li J S and Wan G. 2006. A study on relative radiometric correction of multitemporal remote sensing images. *Journal of Remote Sensing*, **10**(3): 339—344

附中文参考文献

张鹏强, 余旭初, 刘智, 李建胜, 万刚. 2006. 多时相遥感图像相对辐射校正. 遥感学报, **10**(3): 339—344